Chapter 3 – RARE-EARTH-DOPED FIBERS: EXPERIMENT AND MODEL

3.1 INTRODUCTION

Lasers delivering high pulse energies or output power directly from an electronic transition are rare in the mid-infrared region of the spectrum. For that reason we are investigating new materials that could be used as laser media and more particularly as fiber lasers. The choice of the fiber material involves multiple considerations: the maximum phonon energy, the environmental durability, the draw ability and the rare-earth solubility. Fiber lasers operating on laser transitions which have wavelengths > 3 µm need to use glasses with very low phonon energies. ZBLAN fibers have been widely used for fiber laser source emitting below 3 µm. For longer wavelengths, the use of heavier metal fluoride glasses reduces the phonon energies, and therefore, the already demonstrated fluoroindate-based fiber is a good host material candidate for the development of mid-IR fiber lasers.

We chose two rare-earth dopants for the focus of our investigations: dysprosium (Dy^{3+}) and holmium (Ho^{3+}), based on the availability of emission at wavelengths longer than 3 µm. The $^6H_{11/2} \rightarrow {}^6H_{13/2}$ transition of Dy^{3+} corresponds to a wavelength of about 4.3 µm. Lasing has been demonstrated on this transition in crystal hosts [1], but so far only on the shorter wavelength $^6H_{13/2} \rightarrow {}^6H_{15/2}$ transition in fibers [2]. The second candidate, emitting at 3.9 µm, is Ho^{3+}:ZBLAN (ZBLAN : ZrF_4-BaF_2-LaF_3-AlF_3-NaF). The first investigation of this fiber laser used 640 nm pumping and resulted in ~ 1 mW of output power at 3.9 µm [3]. In a second set-up, a 3.4-m long Ho^{3+}:ZBLAN fiber (2000 ppm Ho^{3+}) was used and emitted up to 11 mW on the 3.9 µm transition when pumped at 885 nm with a launched pump power of 900 mW [4]. However, room-temperature operation of Ho^{3+}:ZBLAN on the 3.9 µm transition could not be achieved and the fiber had to be cooled with liquid nitrogen. In order to realize 3.9 µm fiber lasers at room temperature, new host materials are needed that show even lower phonon energies than ZBLAN; fluoroindate may prove suitable.

3.2 SPECTROSCOPY

Contributors to this section: Rita D. Peterson[1], Shrikrishna M. Hegde[2], Francis Théberge[3], Denis Vincent[3], Pierre Mathieu[3]

3.2.1 Dy:fluoroindate Glass

The samples tested here are fluoroindate glasses fabricated by two different companies: Le Verre Fluoré (LVF) and IR Photonics (IRP). The sample from LVF (S/N:110614/3220) was 5 mm in diameter and 10-mm long. The two end faces were optically polished and the cylindrical surface was rough fire polished. The IRP sample (S/N:4000979) had dimensions of 11.54 mm diameter and 9.84 mm length.

The energy-level diagram of the Dy-doped glass samples and their measured absorption spectra are presented in Figure 3-1(a). The most interesting transition is the $^6H_{11/2} \rightarrow {}^6H_{13/2}$ one at 4.2 µm. In Figure 3-1(b) and Figure 3-1(c), we can clearly observe the absorption bands centered around 1.1 µm, 1.3 µm, 1.7 µm, and 2.8 µm. Spectra in (b) are measured with a spectrophotometer UV-Vis-NIR CARY 6000i from AGILENT. Spectra in (c) are measured with a FTIR spectrometer Excalibur FTS 3000MX from DigiLab. The relative absorption ratio between the samples from Le Verre Fluoré (LVF) and IR Photonics

[1] Air Force Research Laboratory, AFRL/RYDH Bldg 620, 2241 Avionics Circle, Wright-Patterson AFB, OH 45433, United States.

[2] University of Dayton Research Institute, Dayton, OH 45469, United States.

[3] DRDC Valcartier, 2459 route de la Bravoure, Québec (Québec) G3J 1X5, Canada.

(IRP) indicates that the Dy concentration was 2.8 times higher in the sample from Le Verre Fluoré. The strongest IR absorption appears at 1280 nm with a weaker, broader mid-IR absorption near 2830 nm. The contribution to phonon absorption begins at ~ 6000 nm and rapidly increases reaching ~ 10 cm^{-1} in these samples. The material thus may be useful up to ~ 6000 nm with further improvements in growth techniques and Dy^{3+} doping concentrations. It also appears that the background absorbance for the lower concentration IRP sample is more than the higher-doped LVF material in the near UV region. The phonon absorption also increases at a shorter wavelength in the IR region in this sample. Assuming the optical polish and surface quality of the two materials are the same, this suggests that the sample growth conditions are different for the two samples and optically, the higher-doped material may be more desirable than the lower doped material.

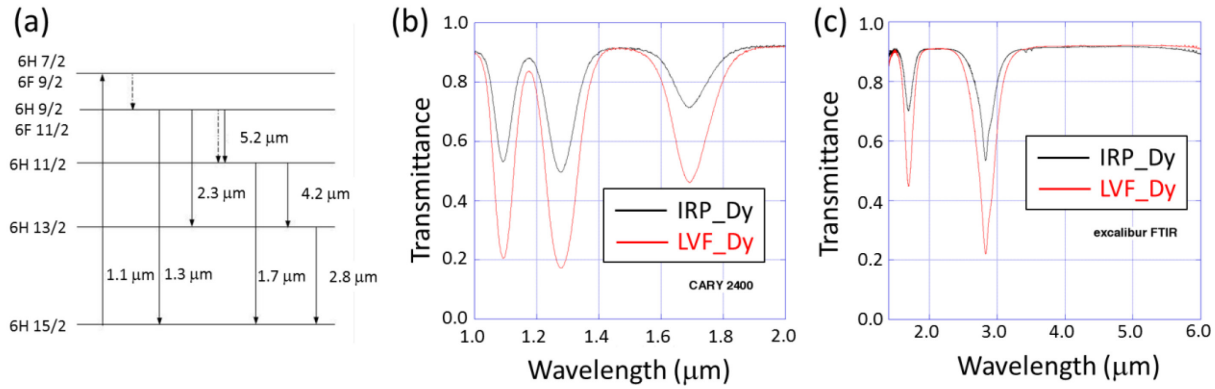

Figure 3-1: (a) Energy-Level Diagram of Dy:fluoroindate Glass; (b) Dy:fluoroindate Absorption Spectra Measured Between 1 µm and 2 µm; and (c) Between 1.5 µm and 6 µm for IR Photonics (IRP_Dy) and Le Verre Fluoré (LVF_Dy) Samples.

Fluorescence in the two Dy:glass samples was measured using a SPEX 220M spectrometer fitted with a liquid N_2 cooled InSb detector and 300 g/mm grating. A Spectra Physics Nd:YVO_4 laser was used to pump the sample. The typical power level used was ~ 400 mW measured at the sample position. A synchronous detection technique using a lock-in amplifier and a mechanical chopper (f ~ 200 Hz) was used to detect the emitted fluorescence in the mid-IR region (2400 nm to 6000 nm). Proper order-sorting longpass filters were used to identify distinct emission peaks. The fluorescence spectra corrected for the spectral response of the system (Figure 3-2), show two peaks at 2900 nm and 5700 nm. The longer wavelength peak at 5700 nm is a second order of the main band at 2900 nm as shown in Figure 3-2. The intensity of the peak is extremely weak, due to the low concentration of Dy in the samples. The expected fluorescence on the $^6H_{11/2} \rightarrow {}^6H_{13/2}$ transition of interest at 4.2 – 4.3 µm cannot be observed at all.

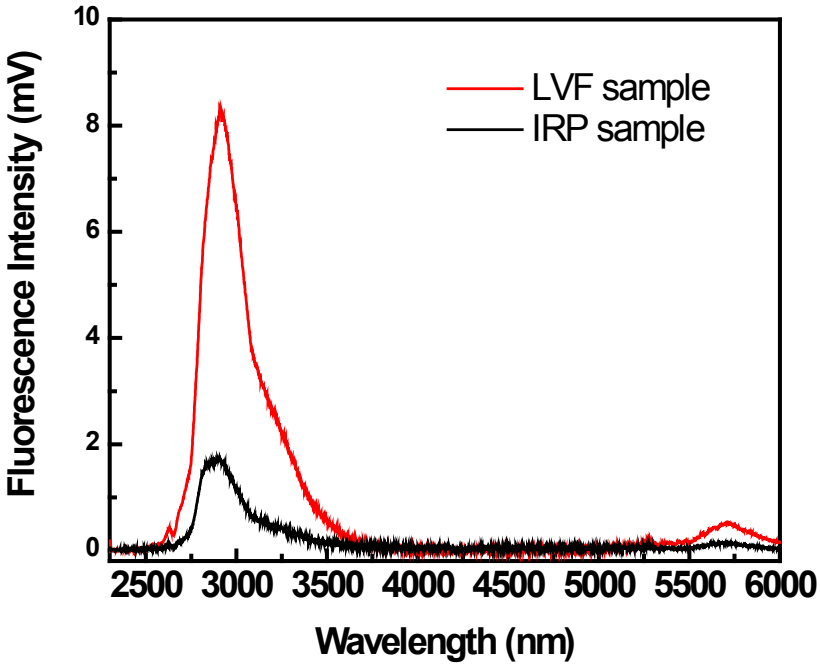

Figure 3-2: Fluorescence in Dy:fluoroindate Glass Samples.

The fluorescence lifetime at different wavelengths was also measured using the set-up presented in Figure 3-3. The Dy-doped glass samples were pumped by 12 ns pulsewidth 1.064 µm Nd:YAG laser. Each fluorescence lines were isolated by coupling the emitted signal into a monochromator. At the output of the monochromator, the lifetime of the isolated fluorescence lines was measured using an InSb detector having a response time of 10 ns.

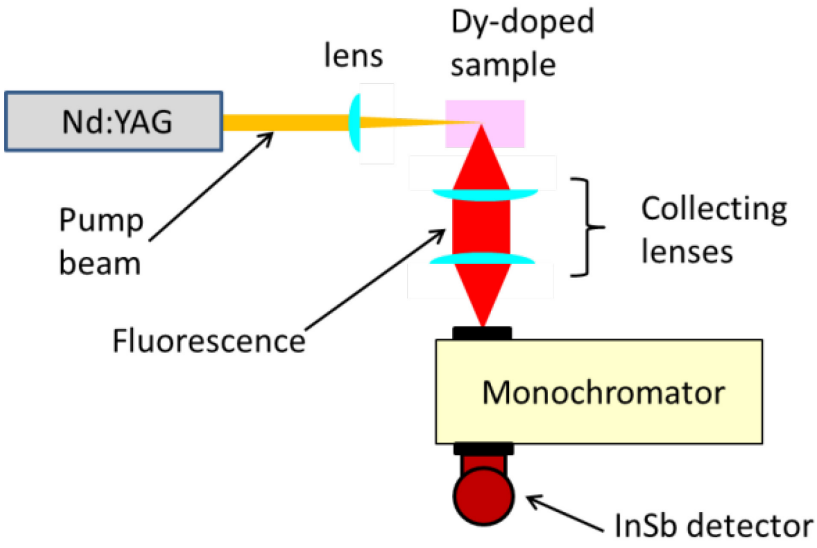

Figure 3-3: Set-Up for Measuring Fluorescence Lifetime of Various Electronic Transitions in Dy:fluoroindate Glass Samples.

The measured fluorescence lifetime at 1.7 µm ($^6H_{11/2} \rightarrow {}^6H_{15/2}$) and at 2.9 µm ($^6H_{13/2} \rightarrow {}^6H_{15/2}$) are presented in Figure 3-4 for both glass samples at room temperature. The measured fluorescence lifetime at 1/e decay was

0.6 ms at 2.9 µm and around 0.9 ± 0.1 µs at 1.7 µm. Once again, using a completely different experimental set-up, no fluorescence was detected around 4.2 µm for the transition $^6H_{11/2} \rightarrow {}^6H_{13/2}$. In order to avoid the coupling loss from the monochromator slits, we replaced this one by a Long Wave Pass Filter (LWPF) transmitting wavelength above 3.3 µm. Although the collection efficiency was increased by more than 10 times, no fluorescence signal around 4.2 µm was detected using the LWPF and the InSb detector for both glass samples at room temperature. The fact that fluorescence at 1.7 µm from the $^6H_{11/2}$ level was detected whereas none was observed at 4.2 µm could be explained by a very low branching ratio for the latter emission. In view of the very short life time of less than 1 µs and the low branching ratio, it seems that lasing from the 4.2 µm transition at room temperature could be difficult to obtain and that it might require operation at much lower temperature.

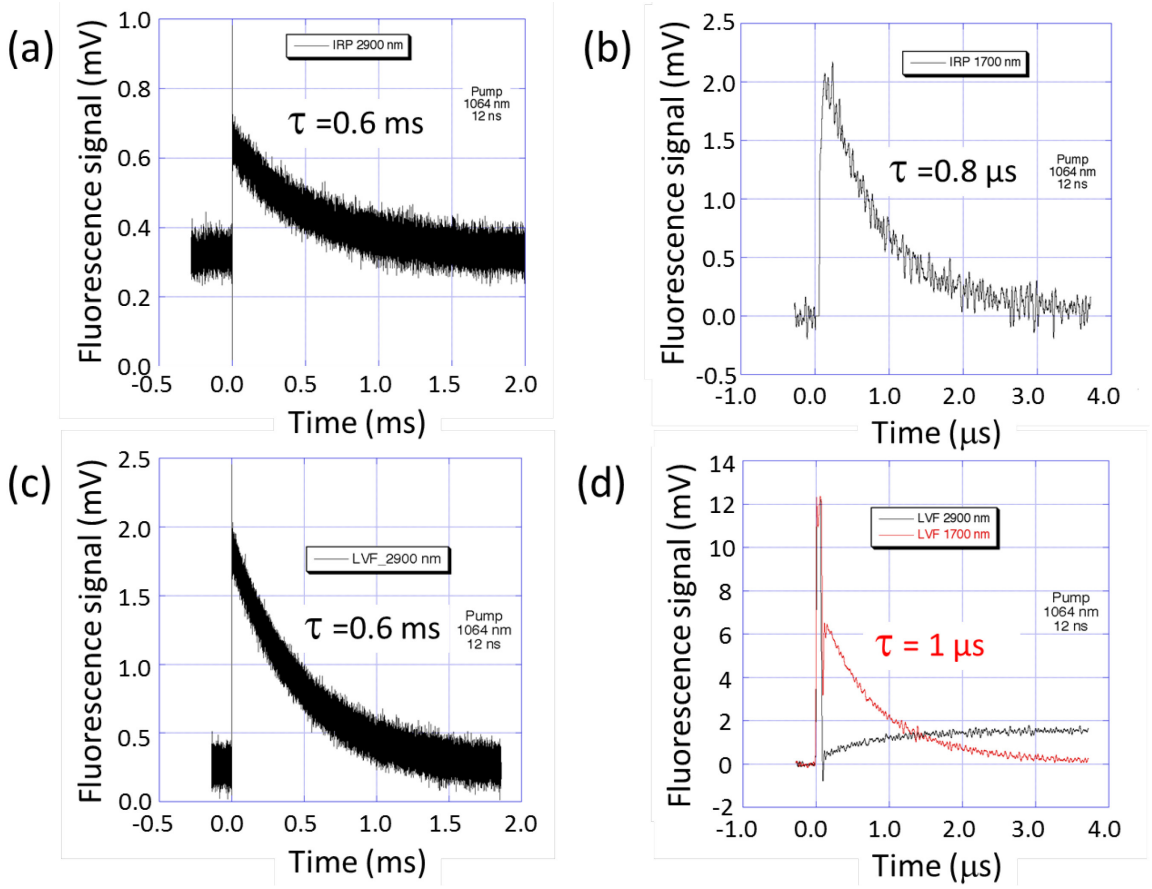

Figure 3-4: Fluorescence Decay for Dy:fluoroindate Pumped by 12-ns Nd:YAG Laser. (a) At 2.9 µm in the *IR photonics* sample (IRP_2900 nm); (b) At 1.7 µm in the *IR photonics* sample (IRP_1700 nm); (c) Fluorescence decay at 2.9 µm in the *Le Verre Fluoré* sample (LVF_2900 nm); (d) At 1.7 µm in the *Le Verre Fluoré* sample (LVF_1700 nm). For comparison, the fluorescence curve at 2.9 µm is superposed in (d) and shows the $^6H_{13/2}$ level being populated by the decay from the $^6H_{11/2}$.

3.2.2 Ho:fluoroindate Glass and Ho:BYF

A single sample of 10% Ho:fluoroindate glass was available for spectroscopic study, in the form of a 10 mm^3 cube, highly polished on all sides. The sample was fabricated by Le Verre Fluoré (LVF), and cut from a larger glass sample, the remainder of which was fabricated into a Brewster-cut sample for lasing experiments, described later in this chapter. Emission experiments were also made on a Ho-doped BaY_2F_8 crystal (Ho:BYF), since we have the means to reproduce lasing experiments in this material, and can use it to

help understand how spectroscopic properties relate to lasing behavior. The BYF host crystal is monoclinic and therefore emission results are polarization dependent. The sample was in the form of a rectangular parallelepiped (~ 4 x 5 x 7 mm^3), with the two 4 x 5 mm^2 end faces optically polished. The Ho concentration was 30%.

Room temperature absorption in the Ho:fluoroindate glass sample was measured using a Cary 5000 dual-beam spectrophotometer. The results are shown in Figure 3-5. Several intense and sharp absorption peaks in the near UV and visible region (300 nm – 650 nm) were observed. Three near IR absorption bands around 750 nm, 1200 nm and 2000 nm were also seen. The visible band around 640 nm showed intense absorption and peak saturation (OD > 10) at 640 nm. Similarly, the near IR band around 2000 nm showed strong absorption and peak saturation (OD > 10) at 1950 nm.

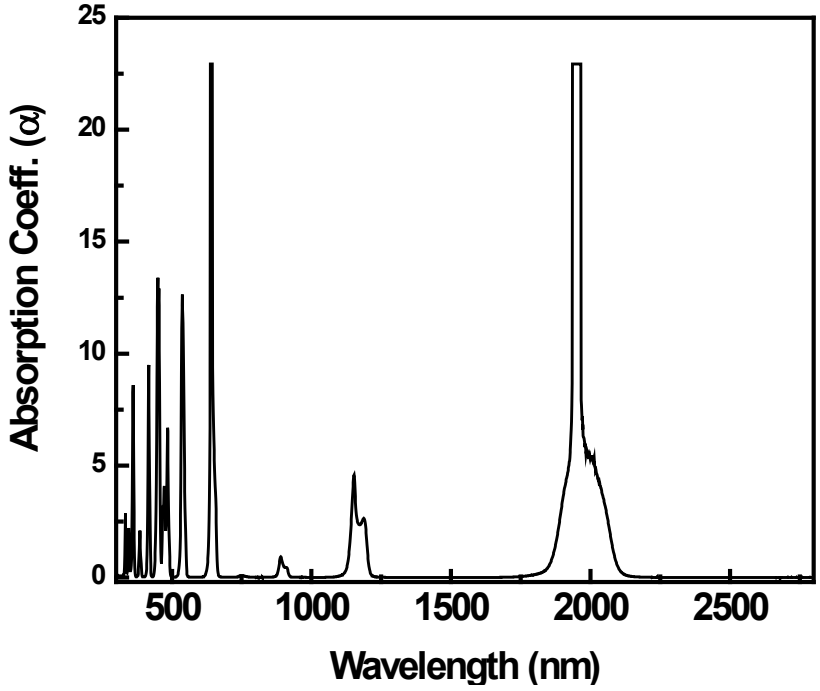

Figure 3-5: Absorption in 10% Ho:fluoroindate Glass Sample.

For measuring emission, a SPEX 220M spectrometer was used, along with a liquid-nitrogen-cooled InSb detector and preamplifier system, in the experimental set-up shown in Figure 3-6. The spectrometer was fitted with a 150 Gr/mm grating blazed at 4 μm. The sample was pumped with a CW Coherent Verdi laser at 532 nm. At this wavelength, the Ho^{3+} absorption is only ~ 45% of the peak absorption at 640 nm. The laser beam was slightly focused on the optically polished end face and emission was collected from the same face in a back reflection geometry. Typical pump power was ~ 500 mW at the sample position. A synchronous detection technique using a lock-in amplifier and a mechanical chopper ($f \leq 200$ Hz) was used to detect the fluorescence. Suitable longpass filters were used to suppress higher orders of the pump and shorter-wavelength emission lines. The room temperature emission spectra for both Ho-doped samples, corrected for the spectral response of the system, are shown in Figure 3-7 and Figure 3-8.

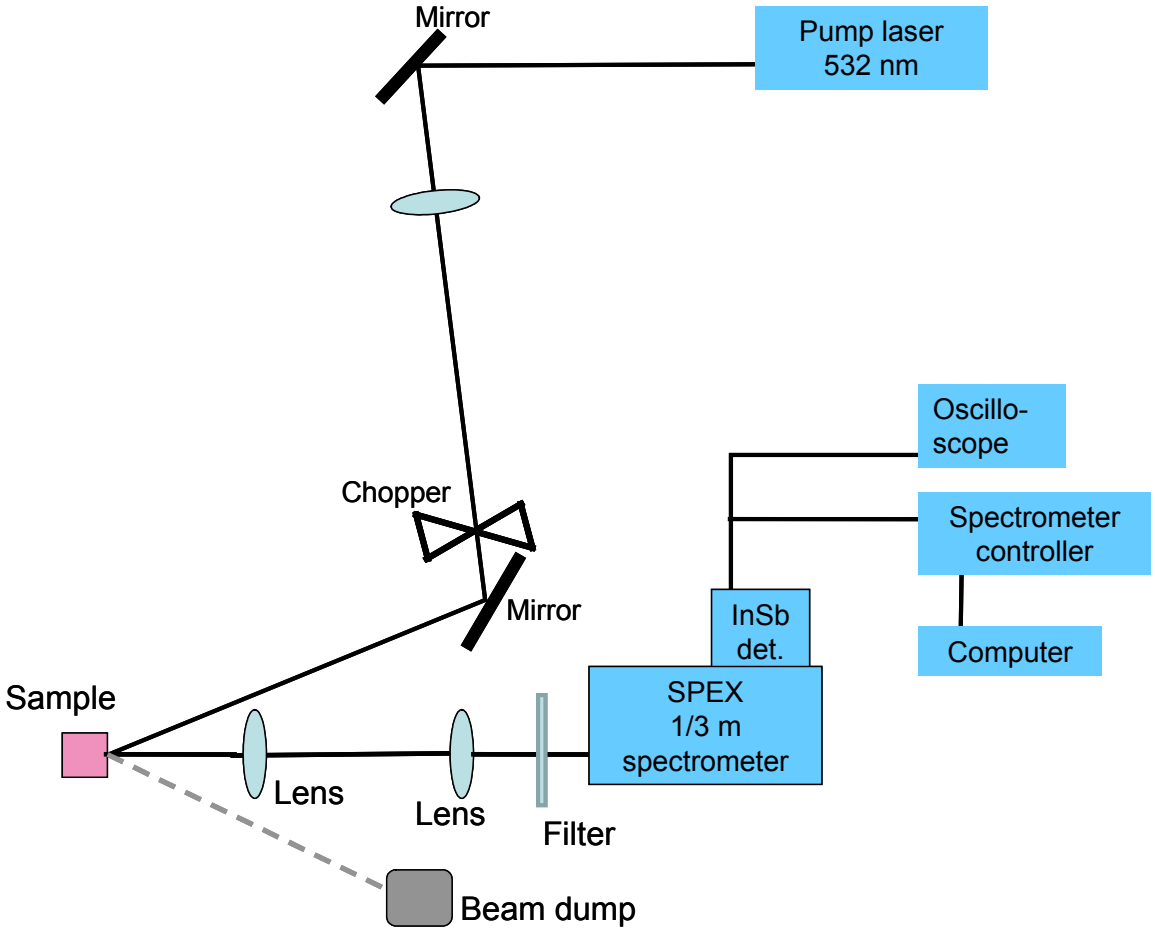

Figure 3-6: Experimental Set-Up for Measuring Emission.

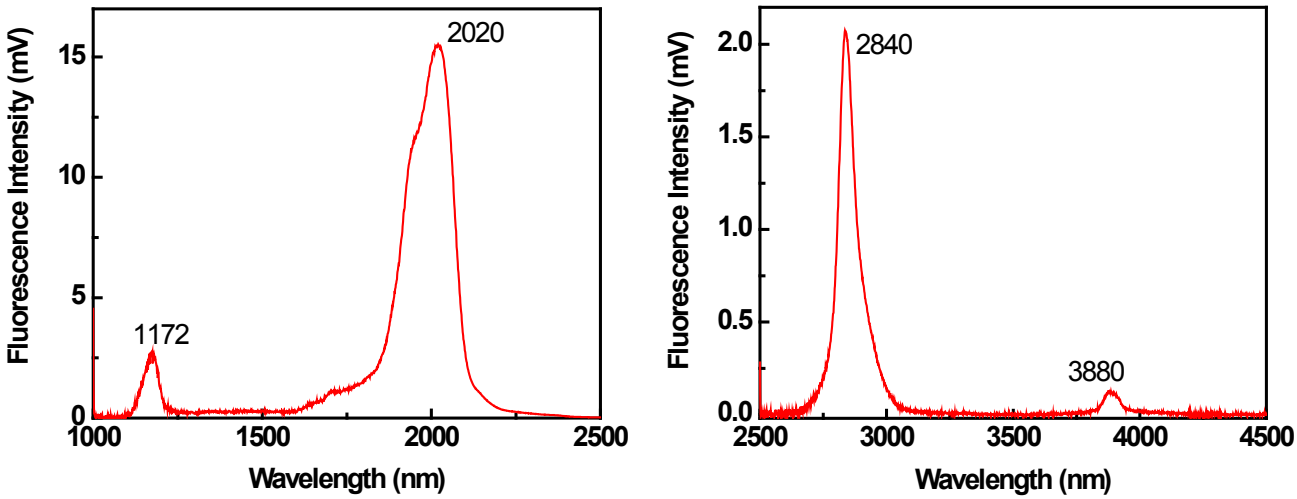

Figure 3-7: Fluorescence in 10% Ho:fluoroindate Glass from 1000 – 2500 nm (Left) and 2500 – 4500 nm (Right).

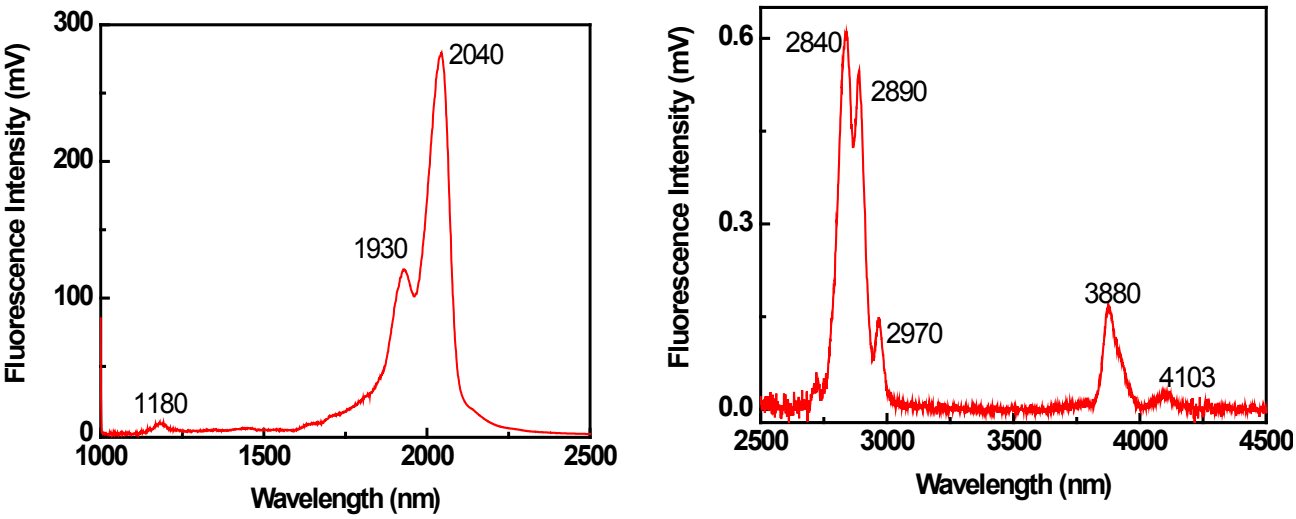

Figure 3-8: Fluorescence in 30% Ho:BYF from 1000 – 2500 nm (Left) and 2500 – 4500 nm (Right).

A number of emission peaks were observed. The strongest by far in both samples was from the $^5I_7 \rightarrow {}^5I_8$ transition around 2020 – 2040 nm, the basis for many highly successful laser systems. Emission from the $^5I_5 \rightarrow {}^5I_6$ transition around 4 μm was considerably weaker than this and the other peaks. The splitting of the peaks seen in the 3000 nm and 4000 nm regions for Ho:BYF is probably due to polarization effects arising from the low symmetry of the host crystal. For experimental simplicity, polarization was not controlled in these experiments.

Fluorescence lifetime was measured in both Ho-doped samples, at room temperature and at 25 K using a helium-cooled cryostat system. The $^5I_5$ lifetime in particular is very short – just tens of μs – so the pump beam was focused near the outside edge of the chopper wheel. The chopper could then be run at its maximum frequency of 200 Hz for measuring this level, giving a pump pulse fall time of less than 10 μs. These results are summarized in Table 3-1.

Table 3-1: Fluorescence Lifetime Data for Ho-Doped Samples at Room Temperature and 25 K.

Level	Ho:fluoroindate RT	Ho:fluoroindate 25 K	Ho:BYF RT	Ho:BYF 25 K
$^5I_5$	30 μs	105 μs	42 μs	58 μs
$^5I_6$	1.3 ms	2.7 ms	2.3 ms	1.1 ms
$^5I_7$	10.6 ms	8.7 ms	20.2 ms	12 ms

The decrease in lifetime in certain cases suggests the influence of up-conversion processes that are favored at low temperature, or possibly even the influence of radiation trapping and reabsorption. To eliminate the latter effect and to obtain more accurate lifetime values, measurements were repeated using a pinhole to limit the pumped area, a method described thoroughly in [5]. The pinhole was placed in the path of the pump beam after the chopper, such that it would be imaged onto the face of the sample by a lens placed between the pinhole and the sample. The pinhole size was varied, changing the area of the sample that was excited. Measured fluorescence lifetime was plotted as a function of pinhole size, shown in Figure 3-9 and

Figure 3-10. The lifetime value t_0 corresponding to a pinhole size of zero was taken to describe the lifetime in the absence of radiation trapping effects, as annotated on each plot.

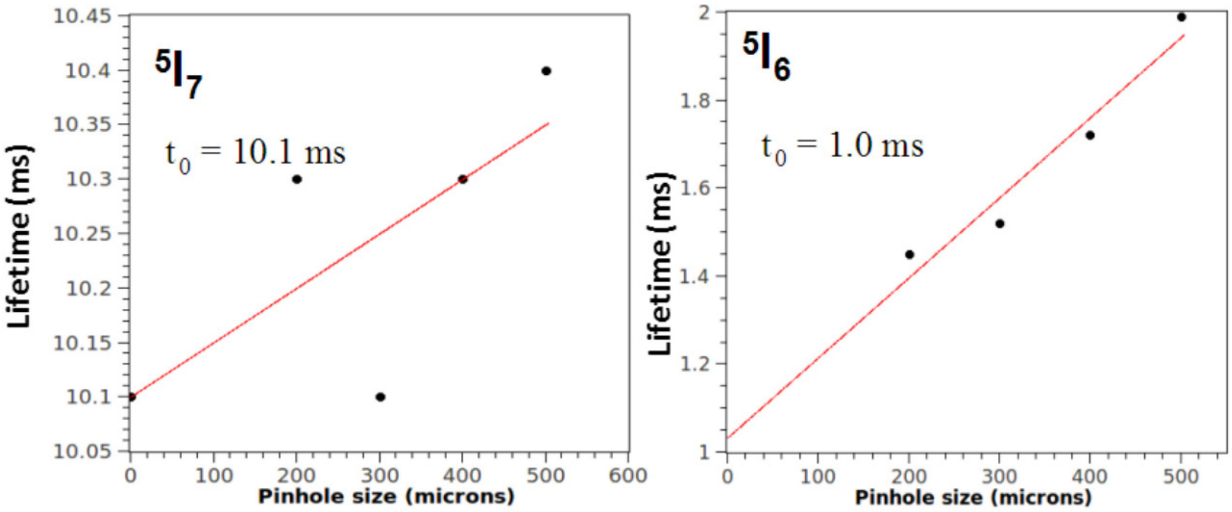

Figure 3-9: Fluorescence Lifetime in Ho:fluoroindate as a Function of Pump Pinhole Size for the $^5I_7$ and $^5I_6$ Levels.

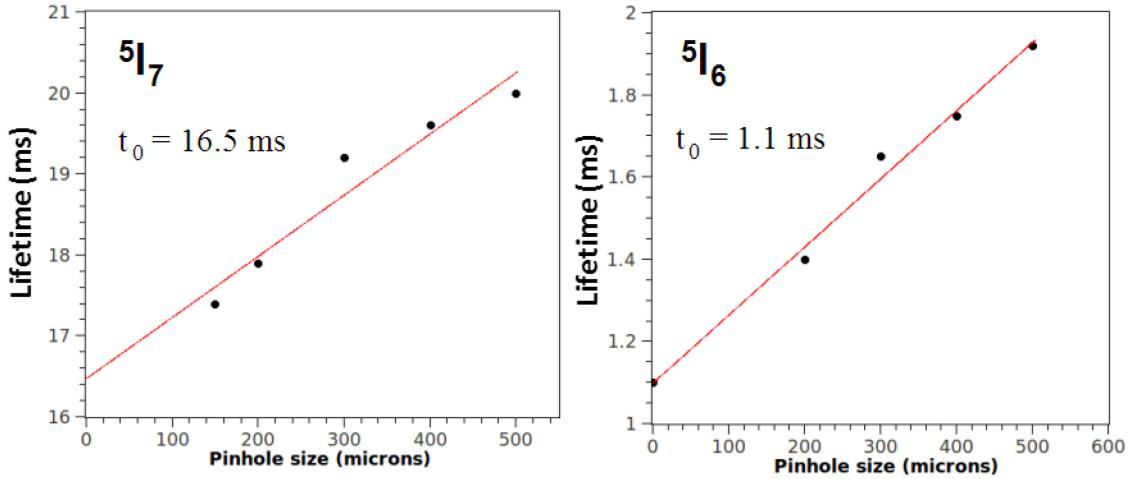

Figure 3-10: Fluorescence Lifetime in Ho:BYF as a Function of Pump Pinhole Size for the $^5I_7$ and $^5I_6$ Levels.

A similar analysis of the critical $^5I_5$ lifetime was attempted but not possible in the current experimental set-up due to excessive noise in the signal for smaller sizes of pinhole. Addressing this and repeating the measurement at low temperature remain incomplete due to unforeseen funding and personnel limitations, and are left as future tasks for a follow-on Task Group, should it decide to continue this line of investigation.

3.3 HO:GLASS MODELLING

Contributors to this section: Espen Lippert[4], Marc Eichhorn[5]

Numerical modelling can be a very useful tool for evaluating new laser systems. This is particularly the case for fiber lasers where the development and manufacturing of the glass fiber itself can be a costly process. The goal of this numerical study has been to evaluate the possibility of designing a Ho^{3+} fiber laser with emission close to 4 µm ($^5I_5$ to $^5I_6$ transition). To make this laser transition efficient it is necessary to use a glass host with low loss (< 1 dB/m) and low phonon energies, to avoid quenching of the laser transition. In this study we have evaluated fluoroindate (fluoroindate) glass as a possible host for a 4-µm Ho laser. In this glass system low loss Ho-doped material is available, but it remains an unanswered question whether or not the lifetime of the $^5I_5$ level is sufficiently long to support continuous laser action under obtainable pumping conditions.

Parameters used in this modeling have been taken from the literature, and some from the spectroscopic measurements described in a previous section. The up-conversion parameters are not easily obtainable and have just been estimated from fitting modeling results to gain-switched laser experiments in Ho:BYF, which is a crystal host with comparable properties.

In order to validate the model it has been applied to Ho laser experiments reported in literature, although they were operating on the 3-µm transition ($^5I_6$ to $^5I_7$).The ability to recreate these results gives greater confidence in the model.

The major challenge in making the 3.9-µm transition in Ho^{3+} lase is depopulating the lower lying manifolds to obtain sufficient gain at the $^5I_5$ to $^5I_6$ transition, which are the second and third exited manifolds in Ho^{3+}. To achieve this, three techniques have been studied:

- Cascade lasing the lower $^5I_6$ to $^5I_7$ transition;
- High doping concentration to achieve beneficial up-conversion; and
- Co-doping to quench the long-lived $^5I_7$ manifold.

High doping concentration and up-conversion is crucial in the operation of Ho:BYF lasing at 3.9 µm, and co-doping and cascade lasing have both previously been applied to Ho:ZBLAN lasers to achieve low threshold and efficient lasing at 2.9 µm. We have investigated whether or not the combination of these three techniques will make it possible to lase the 3.9-µm transition in Ho-doped fluoroindate glass, even with a quite short lifetime of the $^5I_5$.

3.3.1 Model Description

The approach used to model the fiber laser is similar to that used by Quimbye et al. for Dy^{3+}-chalcogenides, and the first test of the model was indeed to recreate his results [6]. The only major difference between his approach and the one used in his work is that we choose to directly integrate the rate equation instead of solving for a steady-state solution.

The lower energy levels of Ho^{3+} together with the pump, fluorescence, stimulated emission, absorption, and up-conversion transitions are shown in Figure 3-11. The ion is modeled as a 4-level system, and the lifetime of the fifth $^5I_4$ level is assumed to be short compared to the others so that the ions converted up to $^5I_4$ end directly up in the $^5I_5$ level.

[4] FFI (Norwegian Defence Research Establishment), P.O. Box 25, NO-2027 Kjeller, Norway.

[5] ISL, French-German Research Institute of Saint-Louis, 5 rue du Général Cassagnou, 68300 Saint-Louis Cedex, France.

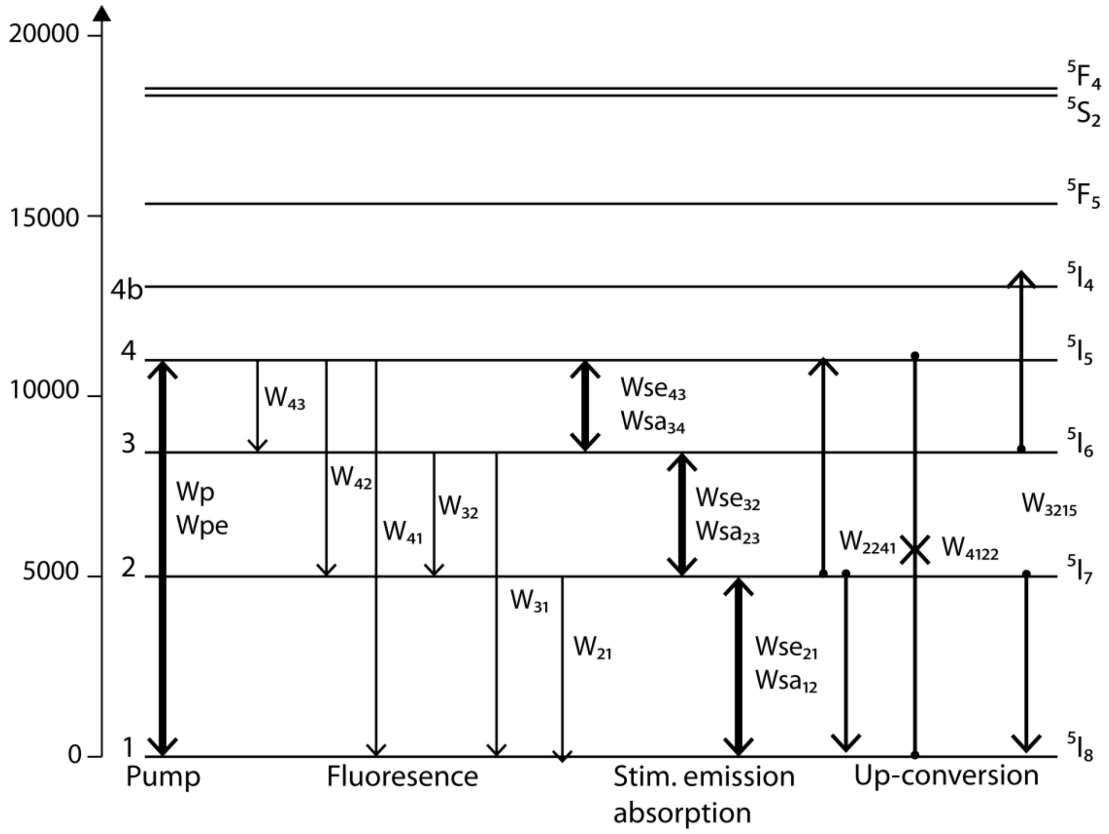

Figure 3-11: Simplified Energy-level Diagram with the Transitions Included in the Model.

The levels and transitions indicated in Figure 3-11 are described by the rate equations in (0.1):

$$\begin{aligned}
\frac{dN_1}{dt} &= -\left(W_{sa12}+W_p\right)N_1+\left(W_{se21}+W_{21}\right)N_2+k_{2241}N_2^{\,2}+k_{3215}N_2N_3-k_{4122}N_1N_4+W_{31}N_3+\left(W_{pe}+W_{41}\right)N_4\\
\frac{dN_2}{dt} &= W_{sa12}N_1-\left(W_{21}+W_{sa23}+W_{se21}\right)N_2-2k_{2241}N_2^{\,2}+2k_{4122}N_1N_4-k_{3215}N_2N_3+\left(W_{32}+W_{se32}\right)N_3+W_{42}N_4\\
\frac{dN_3}{dt} &= W_{sa23}N_2-\left(W_{32}+W_{31}+W_{sa34}+W_{se32}\right)N_3+\left(W_{43}+W_{se43}\right)N_4-k_{3215}N_2N_3\\
\frac{dN_4}{dt} &= W_pN_1+k_{2241}N_2^{\,2}-k_{4122}N_4N_1+k_{3215}N_3N_2+W_{sa34}N_3-\left(W_{pe}+W_{43}+W_{42}+W_{41}+W_{se43}\right)N_4
\end{aligned} \tag{0.1}$$

where $N_i i = 1,2,3$ *or* 4, are the population densities, W_{saij} and W_{seij} are the rates of absorption between level i and j, W_{ij} are the transfer rates between level i and j, and k_{ijkl} are the coefficients for the up-conversion processes.

When the new population has been found by integrating the rate equation over a desired time step, the gain for each section along the fiber is calculated by integrating the difference between the absorption and emission over the transversal mode, which is assumed to be Gaussian with a radius calculated from the fiber core size and NA. Using this calculated gain, the power distribution along the fiber is shifted one step in the fiber. This new power distribution is then used in solving the rate equations in a new iteration. This continues until the solution is stable. Finding a steady-state solution using this direct integrating method can be time consuming due to the oscillatory nature of the problem; this can be helped by scaling the rate equations without changing the steady-state solution, which can be achieved by scaling down the population and compensating by scaling up the cross-sections, and up-conversion rates.

3.3.2 Validation of Model

In order to gain confidence in the numerical model, it was validated by applying it to experiments reported in literature. The fiber material used in these experiments was ZBLAN, which is a fluoride material with comparable properties to fluoroindate. The parameter values used in these validations give guide lines for what could be reasonable values for fluoroindate, but they are not directly used in the fluoroindate model. The experiments we chose were lasers on the 2.9-µm transition ($^5I_6$ to $^5I_7$), and although our aim was to obtain lasing on the 3.9-µm transition ($^5I_5$ to $^5I_6$) the model's ability to recreate these experiments will show that the lower levels are modelled correctly.

The first experiment we modelled was reported by Jackson [7]. It is simple to model in the sense that it pumped directly to the upper laser level ($^5I_6$), and the lower laser level ($^5I_7$) is depopulated by co-doping with Pr^{3+}, which effectively reduces the lifetime of the lower laser level to probably on the order of 100 µs. The parameters used in the model are shown in Annex A. This results in an efficient laser with very low threshold. The experimental points and the model fit shown in Figure 3-12 are in good agreement. We also tried to vary the parameters in the simulations, such as lifetimes and cross-sections, and found that the results were very insensitive to this. This is reasonable since the threshold is very low and the slope is limited by the quantum defect and the ratio of output coupling to total loss. Although the fit was insensitive to some parameter values the fit show that the model can give reasonable results.

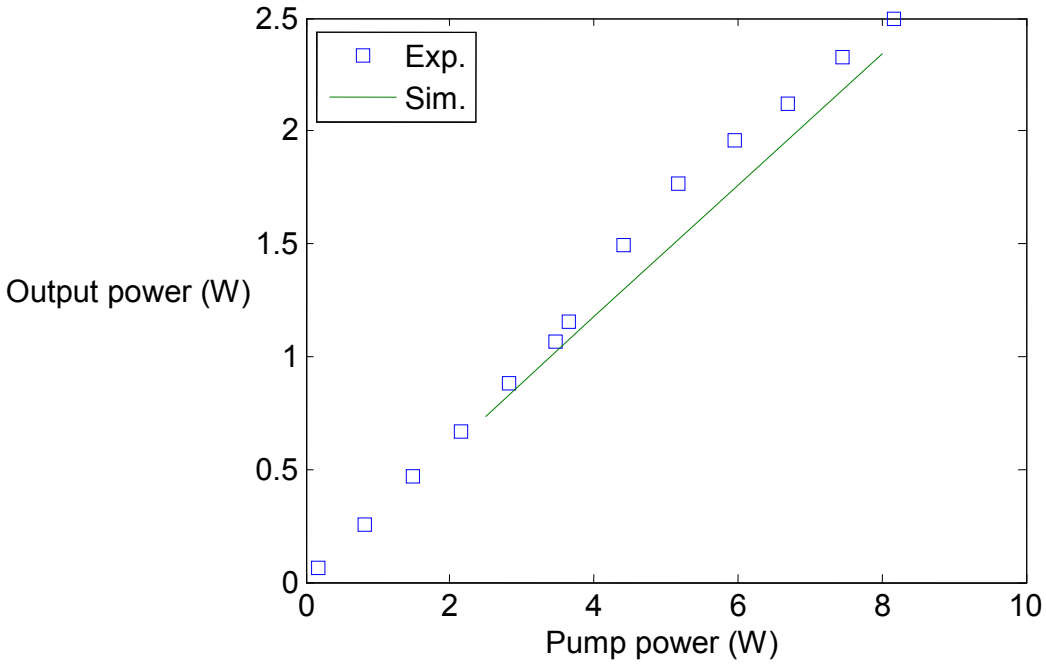

Figure 3-12: Model Fit to 2.94 µm Ho:ZBLAN Fiber Laser.

The second experiment used in the model validation was more challenging. The laser was also a Ho:ZBLAN laser, but without Pr^{3+} co-doping. Instead the $^5I_7$ level was depopulated through cascade lasing of the 2-µm transition [8]. This laser had a much more complex behavior and high threshold. The parameters used are shown in Annex A. The result of the model fit is shown in Figure 3-13.

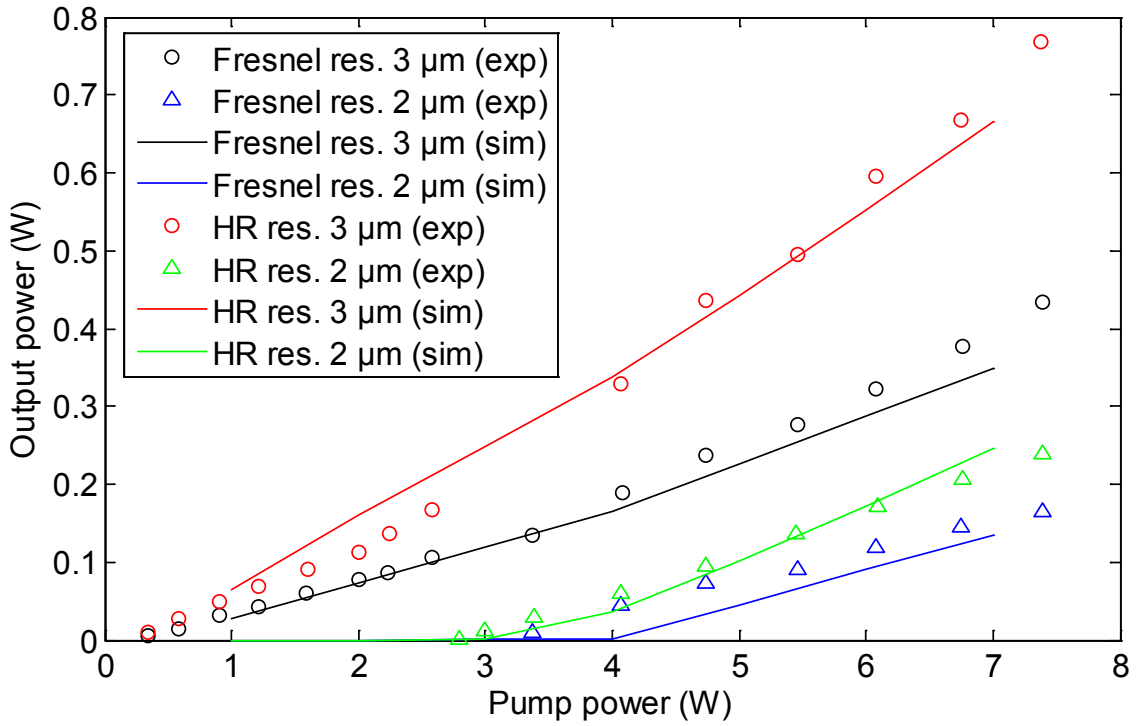

Figure 3-13: Model Fit to Cascade Lasing in Ho:ZBLAN.
Two sets of resonator mirrors were applied to the fiber laser.

As Figure 3-13 shows, the fit between the model and the experiments are not as good as for the previous case, but still much of the behavior is recreated. This example is much more sensitive to the input parameter values, and making the model fit the experiment reasonably well greatly adds to the confidence that it can model the behavior of a cascade fiber laser system.

3.3.3 Model Predictions

Lasing the 3.9-µm transition in Ho^{3+} is challenging even without lifetime quenching from the phonon coupling. The lifetime of the $^5I_5$ level is shorter than that of the $^5I_6$ level, which in turn is shorter than the $^5I_7$ lifetime, and the substantial non-radiative transfer only makes this situation worse. These unfortunate lifetime ratios inhibit population inversion between the manifolds. Even though this can be overcome to some extent by lasing to a level high up in the lower lying manifold, it tends to be very difficult to make transitions to these high lying levels lase in continuous operation for feasible pump intensities. There is only one demonstration of lasing the 3.9-µm transition continuously in a fiber laser, and they achieved only 11 mW and had to cryogenically cool the fiber to 77 K [9]. To mitigate this lifetime problem, some mechanism had to be found to depopulate the $^5I_6$ level. The obvious way to do this is to lase both the 3.9-µm and the 2.9-µm transition simultaneously. If the threshold of the 2.9-µm transition can be made low, the population in the $^5I_6$ level can be kept down, thus allowing for a more favorable population ratio. A second effect which not only depopulates the $^5I_6$ level, but also repopulates the $^5I_5$ level is the up-conversion from both the $^5I_6$ and $^5I_7$ level, as indicated by Figure 3-11. This effect will increase with increasing doping concentration, making the doping level an important parameter in the design of a Ho:fluoroindate fiber laser. A challenge with the cascade lasing scheme is that the lower level of the 2.9-µm transition ($^5I_7$) also has a longer lifetime than the upper level ($^5I_6$). It has been shown, however, that this transition can lase in spite of this to lines high up in the $^5I_7$ manifold. It has also been shown that depopulating this level, e.g. using co-doping like in the first validation experiment, will reduce the threshold of the 2.9-µm transition.

This simple analysis led us to investigate two approaches to make the Ho-fiber laser at 3.9 µm, both using cascade lasing at the 2.9-µm transition, but one with co-doping to reduce the lifetime of the $^5I_7$ level and one without.

It is also clear that having high pump intensity is advantageous, and therefore we chose a fiber structure where the pump core was as small as possible, but still large enough to allow pumping with high brightness laser diodes. We chose to investigate a dual-cladding fiber with an inner core with a 10-µm diameter and an outer pump core of 50 µm. We applied dual-end pumping with 10 W launched pump power in both directions at 895 nm. In the model we used the up-conversion coefficient estimated from the Ho:BYF model fit reported by Eichhorn, and we further assumed that these coefficients will be proportional to the doping concentration [10]. The assumption of linearity has been shown to be valid at least for low doping concentration (< 4 mol %) [11]. Our values were estimated for ionic distances equal to that of 10% doping in fluoroindate and are most accurate around this concentration, but will probably not overestimate the up-conversion at lower concentration. The lifetimes we used were the ones we determined experimentally, which were considerably shorter than what we had hoped when this host material was chosen for investigation. We used the absorption and emission experiments to estimate the energy levels of the laser manifold and the shape of the emission lines. The rest of the parameters were estimated from literature values of Ho^{3+} in similar hosts [12]. Where the values were uncertain, conservative estimates were used. A list of the parameters is given in Annex A.

The results from the modeling of the Ho-doped double-clad fiber are shown in Figure 3-14 and show that for high doping concentrations the 3.9-µm transition lases efficiently even with a very short lifetime of 30 µs assumed for the $^5I_5$ level. Using 20% Ho doping the optical efficiency is ~ 40%, which is almost twice the ratio of pump wavelength to laser wavelength, usually limiting the efficiency of an optically pumped laser. The reason for this is that the electrons are recirculated by the strong up-conversion from the $^5I_6$ and $^5I_7$ levels, and can contribute to laser action several times. This process greatly reduces the detrimental effect of the short lifetime of the $^5I_5$ level. Even though the long lifetime of the $^5I_7$ level reduces the efficiency of the 2.9-µm transition, co-doping to mitigate this does not help since this also reduces the efficiency of the up-conversion recirculation. Only for the lowest doping concentration, where the up-conversion is less important, is the co-doping beneficial.

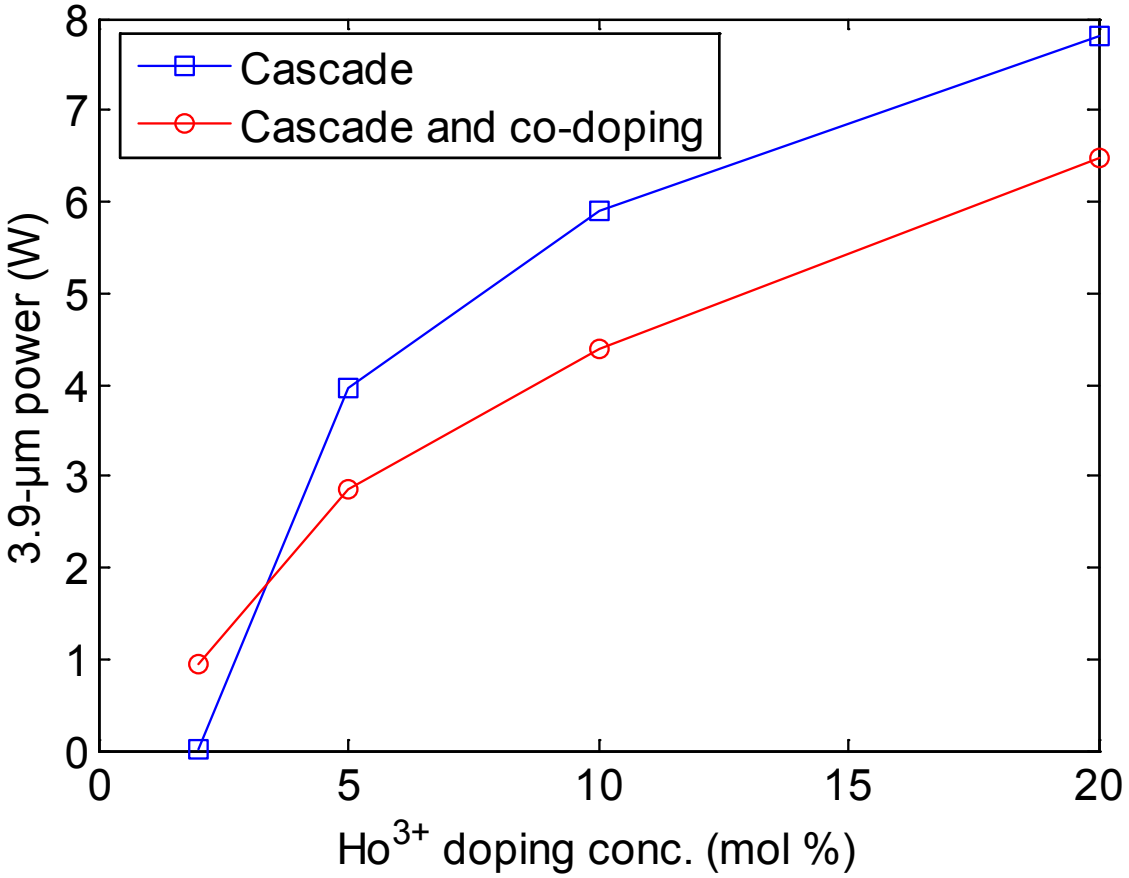

Figure 3-14: Model Predictions of Two Cases of Cascade Lasing a Double Clad Fiber, Pumped by Two 10 W Pumps, With (Red Curve) and Without Co-Doping (Blue Curve) for Varying Doping Concentrations.

To study the effect of the $^5I_5$ lifetime we varied the lifetime. The results in Figure 3-15 show that at this pump level with this fiber geometry the efficiency is saturated already at a lifetime of 100 µs. This shows that the modeled up-conversion processes are very efficient in re-circulating the electrons which undergo non-radiative or radiative transfer to the $^5I_6$ and $^5I_7$ levels. The only lost energy in the system is across the $^5I_7$ to $^5I_8$ transition, which takes place in the up-conversion process.

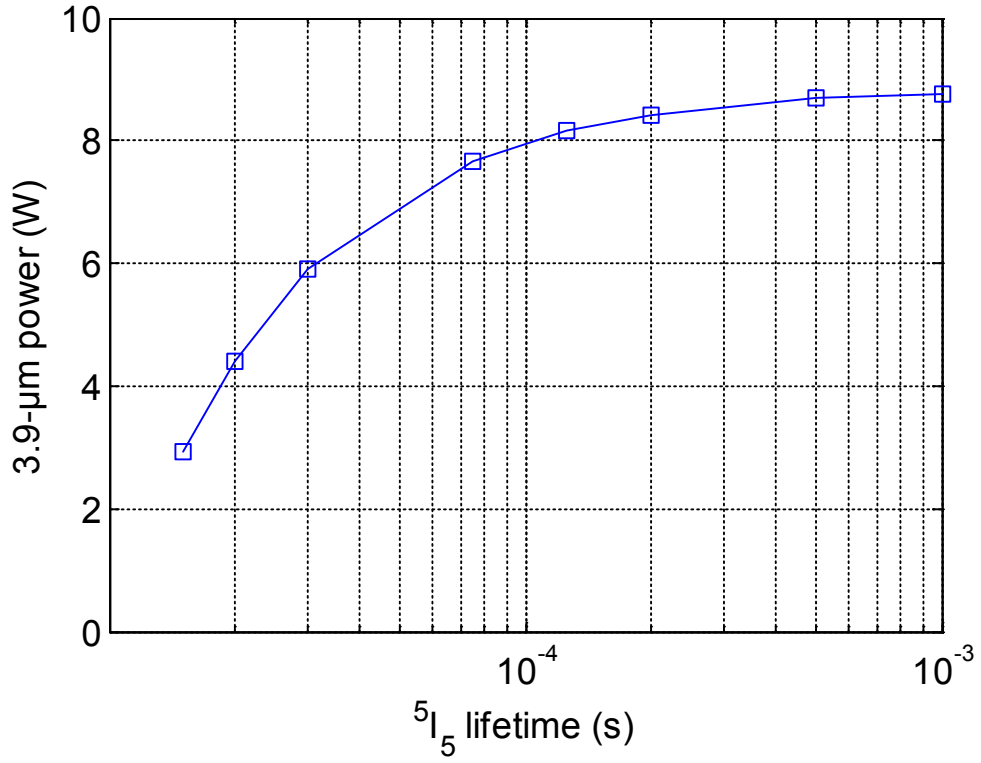

Figure 3-15: Output Power at 3.9 µm from a Fiber with 10 mol % Ho^{3+}, for Varying Lifetime of the $^5I_5$ Level.

3.3.4 Conclusions

We have shown that a double-clad Ho-doped fluoroindate glass fiber can be lased efficiently at 3.9 µm for doping concentrations greater than ~ 5 mol %, provided that the up-conversion coefficients we have used are correct. It should be noted, though that the values we have used have been extracted from model fitting in a different crystalline host (BYF), and that more work should be done on extracting better values for emission cross-sections and up-conversion coefficients. The peak emission cross-sections should be easily available from Judd-Ofelt analysis, whereas the up-conversion coefficients can be estimated from model fitting to fluorescence measurements under strong pumping. If the true values are similar to what we have assumed, it should be feasible to design an efficient diode pumped 4-µm fiber laser.

3.4 HO:GLASS LASING

Contributors to this section: Marc Eichhorn[6], Christelle Kieleck[6], Antoine Berrou[6]

Like Ho:ZBLAN, Ho^{3+}:fluoroindate glass exhibits an absorption peak around 890 nm (Figure 3-16). Thus we need an intense pump source at this wavelength. We will use Cr^{3+}:LiSAF laser to pump, as a first demonstration, a bulk Ho^{3+}:fluoroindate glass. In this sub-section we present first the characteristics of the Cr^{3+}:LiSAF laser that was used as pump source. In order to compare the performance of our new material (Ho^{3+}:fluoroindate glass) to well-known materials, we built a laser based on a Ho^{3+}:BYF crystal. Its performance is reported thereafter. Replacing the Ho^{3+}:BYF crystal by Ho^{3+}:fluoroindate glass in the laser cavity we recorded, to the best of our knowledge, the first laser activity of this glass.

[6] ISL, French-German Research Institute of Saint-Louis, 5 rue du Général Cassagnou, 68300 Saint-Louis Cedex, France.

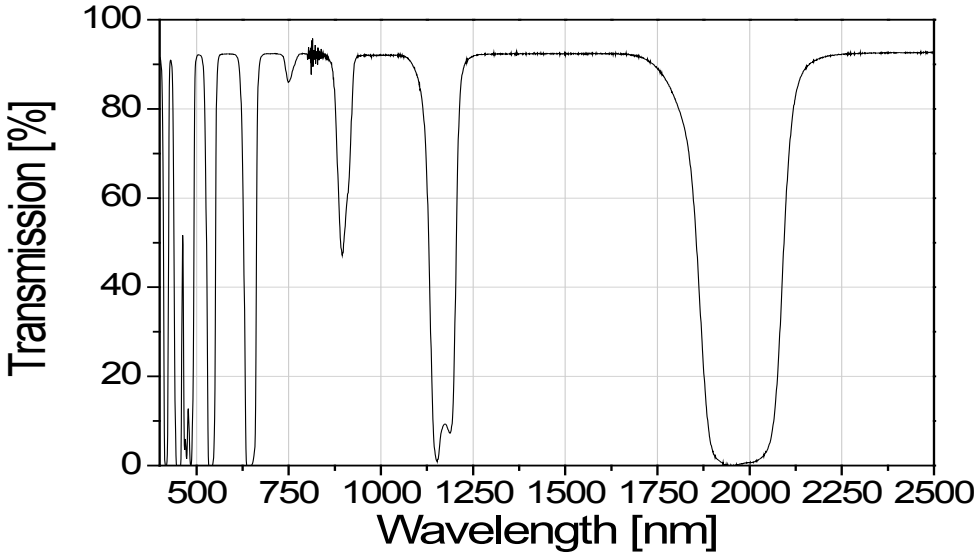

Figure 3-16: Transmission of Uncoated Ho^{3+}:fluoroindate Glass as Function of Wavelength.

The experimental set-up of the Cr^{3+}:LiSAF (Cr^{3+}:$LiSrAlF_6$) laser is presented in Figure 3-17. The crystal rod is 101.6-mm long and 6 mm in diameter. The chromium doping concentration is 0.8%. It is flash lamp-pumped, resulting in available pump energies for holmium pumping of several joules at pulse widths of ~ 80 µs in free-running mode. In order to obtain a narrow emission linewidth from the laser, a threefold SF4-prism monochromator was inserted into the cavity, resulting in a linewidth of 2.5 nm, centered at 889 nm.

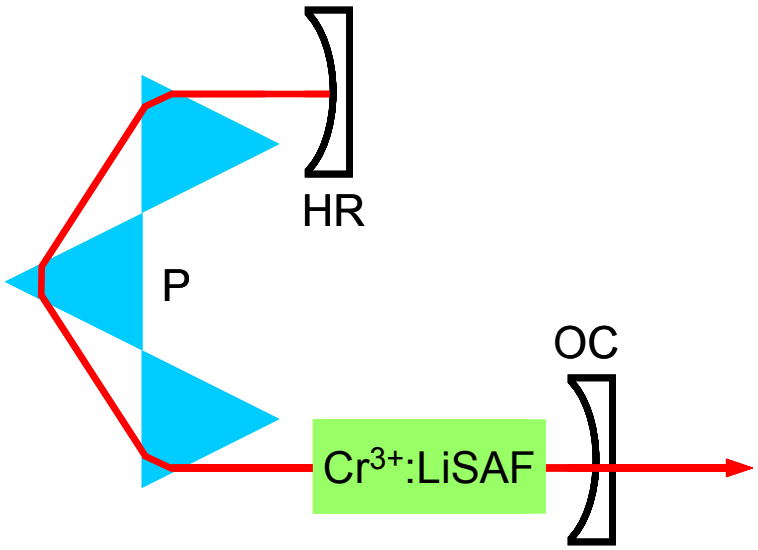

Figure 3-17: Cr^{3+}:LiSAF Laser Layout. HR: High Reflectivity Mirror; P: Prisms; OC: Output Coupler.

The laser output energy as function of the electrical flashlamp energy is reported in Figure 3-18. The laser set-up is presented in Figure 3-19. Ho3+:BYF crystal is 15-mm long, it is not coated therefore its faces are cut off with an angle to reduce the Fresnel loss. It is pumped from both sides and its temperature is not controlled. As the pump source beam is polarized, we used a polarized beam splitter to separate the pump

beam into two parts. The ratio between the two arms can be controlled with the half-wave plate 1. The pump beam is focused inside the crystal using plano-concave lenses. The laser cavity which is approximately 250-mm long is composed of three mirrors. The dichroic mirrors M1 and M2 are highly transmissive for the pump beam and highly reflective for the laser beam. The output coupler M3 has a reflectivity of 80%. Maximum output energy of 650 mJ was achieved at 150 J electrical energy. The conversion slope efficiency was measured to be 0.63%, which is lower than what we obtained few years ago with this laser [10].

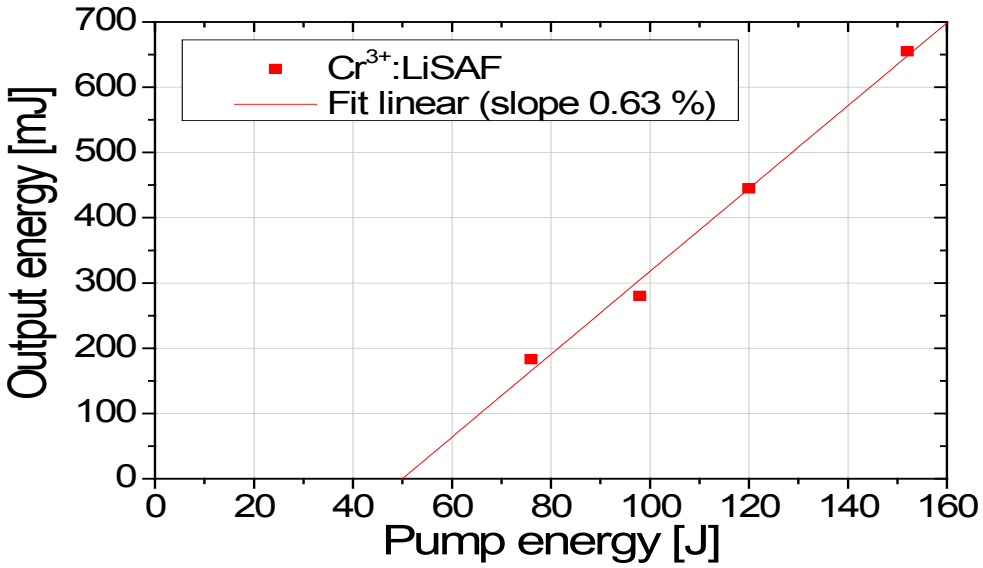

Figure 3-18: Cr^{3+}:LiSAF Laser Output Energy as Function of Electrical Flashlamp Energy (80 µs Pulse Duration).

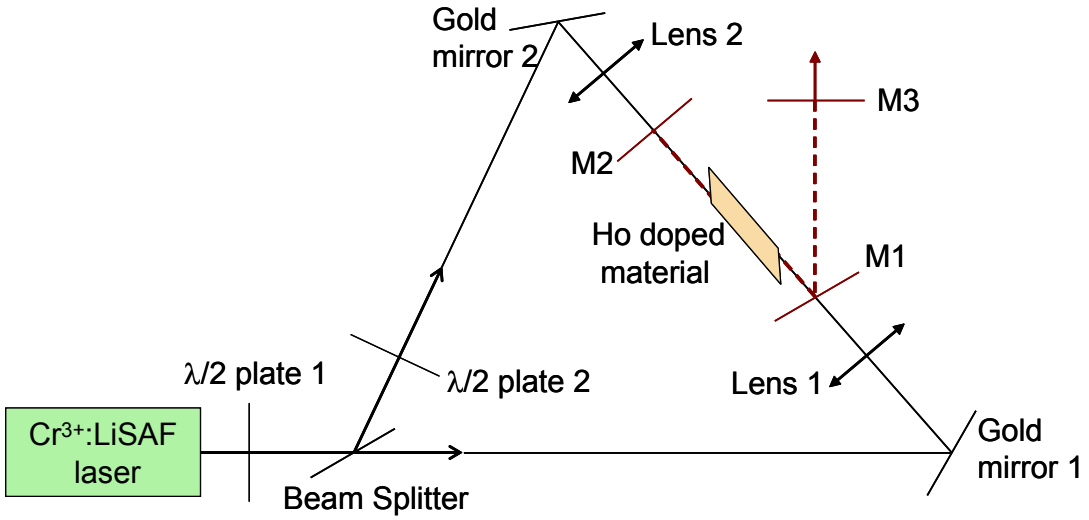

Figure 3-19: Mid-Infrared Laser Set-Up.

Ho3+:BYF crystal (Ho:BaY2F8) is an interesting material because it can be pumped in the near-infrared at 889 nm and emit in the mid-infrared at 3.9 µm. Due to the longer lifetime of the terminating level compared to the upper laser level, this transition can be regarded as a quasi-three-level transition. Moreover due to the strong difference in upper and lower-state lifetimes (52 µs and 5.45 ms respectively), the laser can be

operated efficiently only in pulsed mode with repetition rates smaller than the inverse lower level lifetime. However, when strongly doped with Ho^{3+} (> 20%) an Energy Transfer Up-conversion (ETU) process allows for recycling of used inversion and thus can allow for cw operation [10]. Here, we only run the pump source in single shot (80 µs pulse duration).

The laser output energy as a function of the pump energy is reported in Figure 3-20. Three different pump conditions were examined. First, in blue, we roughly separated the pump beam into equal parts. Then, in green, we rotated the half-wave plate 1 for maximum pump energy in the first arm. Finally, in red, we blocked the pump beam of the second arm. The evolution of the slope efficiency between the three curves shows that the second arm pumping is less efficient than the first arm. We need more investigations to determine the cause of this behavior. Nevertheless we obtained a threshold energy of 125 mJ, a slope efficiency of 6.9% and maximum output energy of nearly 35 mJ at 650 mJ pump energy. The temporal profile of the laser beam in Figure 3-21 shows a quasi-continuous emission after spikes at the beginning. This behavior is well explained with numerical simulation in [10].

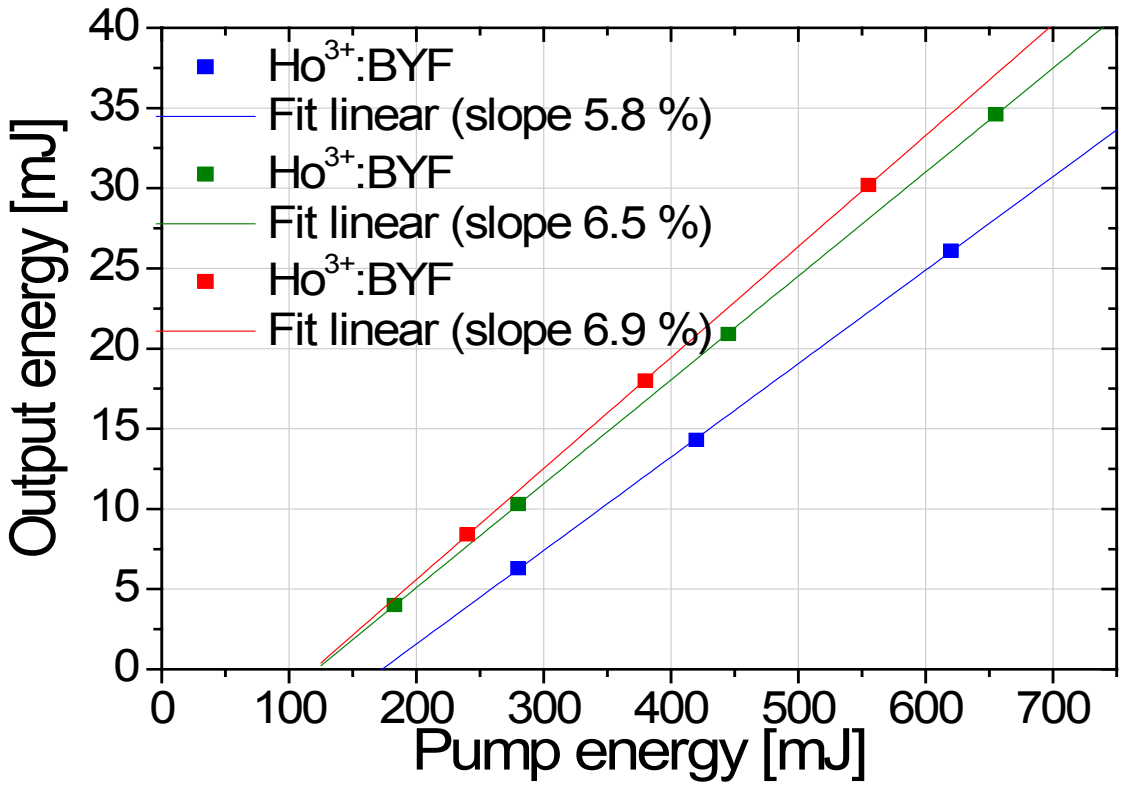

Figure 3-20: Ho^{3+}:BYF Output Energy as Function of Cr^{3+}:LiSAF Energy for Three Different Repartitions of Pump Intensity Between the Two Arms: 57% in the First Arm and 43% in the Second (Blue); 85% in the First Arm and 15% in the Second (Green); and 100% in the First Arm (Red).

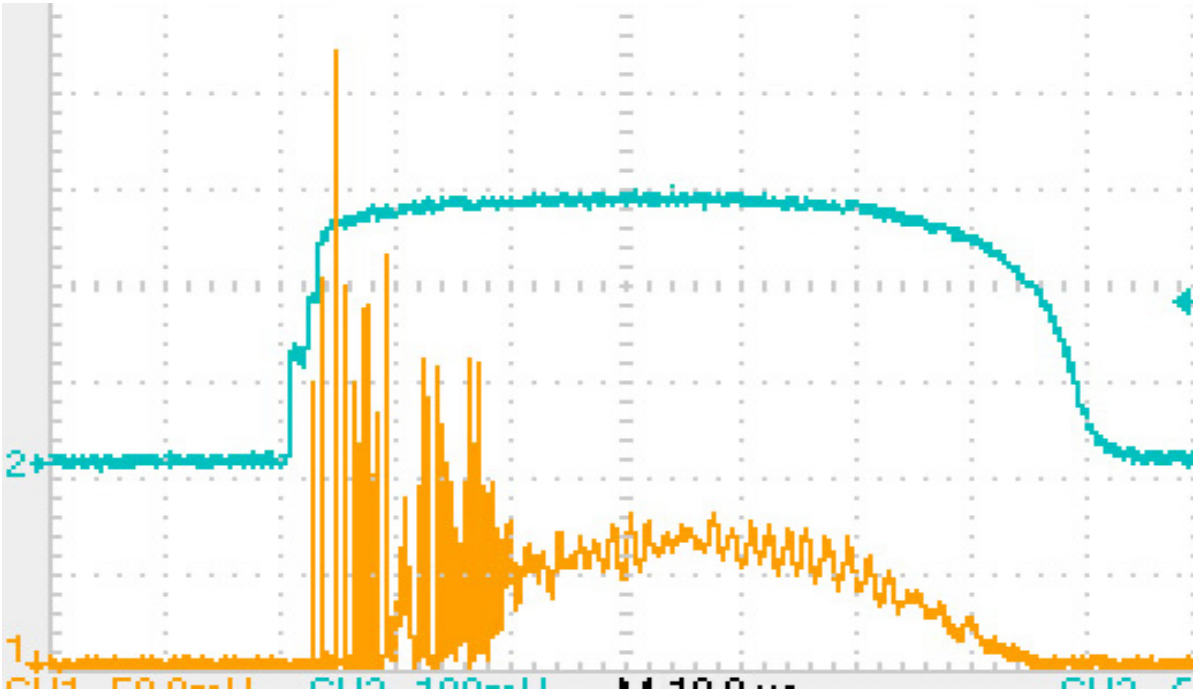

Figure 3-21: Temporal Profile of Cr^{3+}:LiSAF Laser Pulse (Cyan) and Ho^{3+}:BYF Laser Pulse (Orange) at Maximum Output Energy.

A picture of our Ho^{3+}:fluoroindate glass is presented in Figure 3-22. It shows high optical quality (bulk) and surface finish. It is 30-mm long and has a holmium doping concentration of 10%. Like the Ho^{3+}:BYF crystal, it has no optical coating. Thus it is Brewster cut to limit the Fresnel loss.

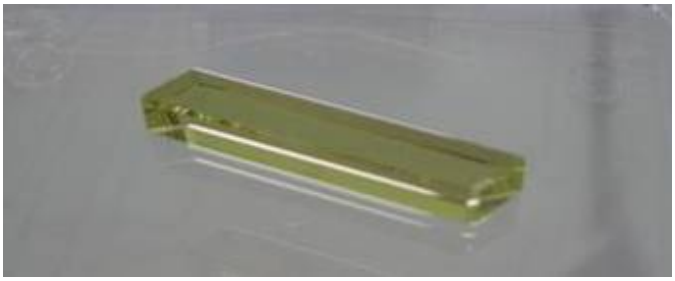

Figure 3-22: Ho^{3+}:fluoroindate Glass.

We used the set-up presented in Figure 3-19, replacing the Ho^{3+}:BYF crystal with this fluoroindate glass. Since this glass is two-times longer than the BYF crystal, we needed to realign the pump and the cavity. The laser output energy as a function of the pump energy is reported in Figure 3-23. We recorded the output energy for two configurations. The first configuration was with 85% of the pump energy in the first arm and the remaining 15% in the second one. For the second configuration we blocked the pump of the second arm, keeping the same power in the first arm. The laser threshold energy was approximately 230 mJ. The conversion slope efficiency was 1.3% with 5.4 mJ maximum output energy. It appears that this laser is not as efficient as the Ho^{3+}:BYF laser, but we must emphasize that the laser cavity was almost the same for the two lasers therefore it was not optimal for the second experiment with a longer active medium.

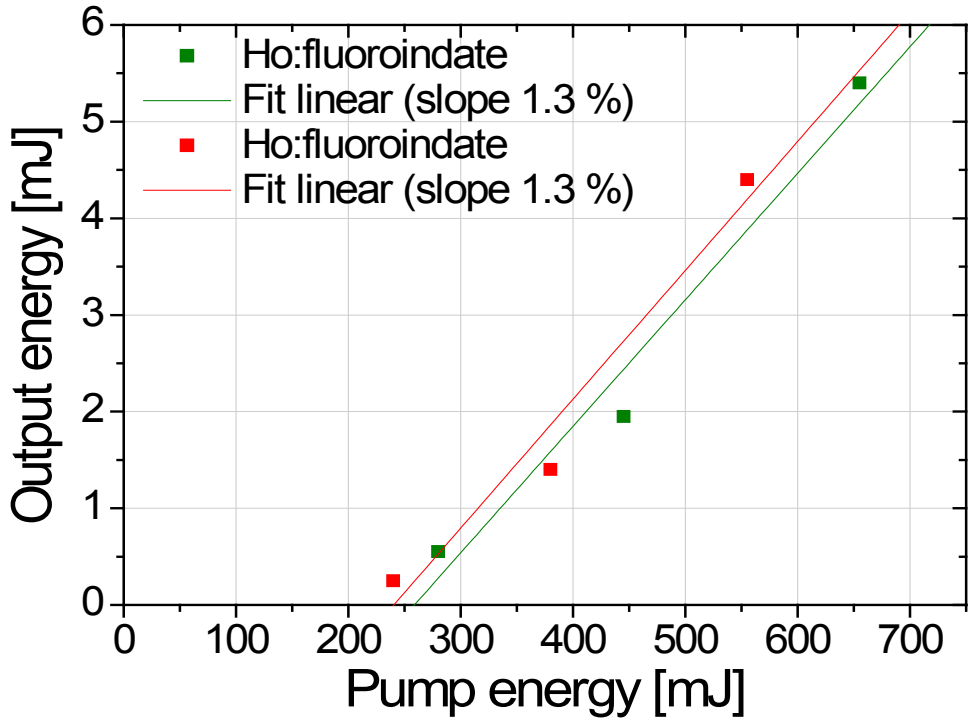

Figure 3-23: Ho^{3+}:fluoroindate Output Energy as Function of Cr^{3+}:LiSAF Energy for Two Different Repartitions of the Pump Energy Between the Two Arms: 85% in the First Arm and 15% in the Second (Green) and 100% in the First Arm (Red).

The temporal profile of the Ho^{3+}:fluoroindate laser beam at maximum output energy is reported in Figure 3-24. This profile shows separated spikes for 30 µs and then nearly quasi-continuous emission with weak power during 20 µs. This behavior is expected when pumping few times above threshold and is comparable to Ho^{3+}:BYF laser beam profile at this laser energy level.

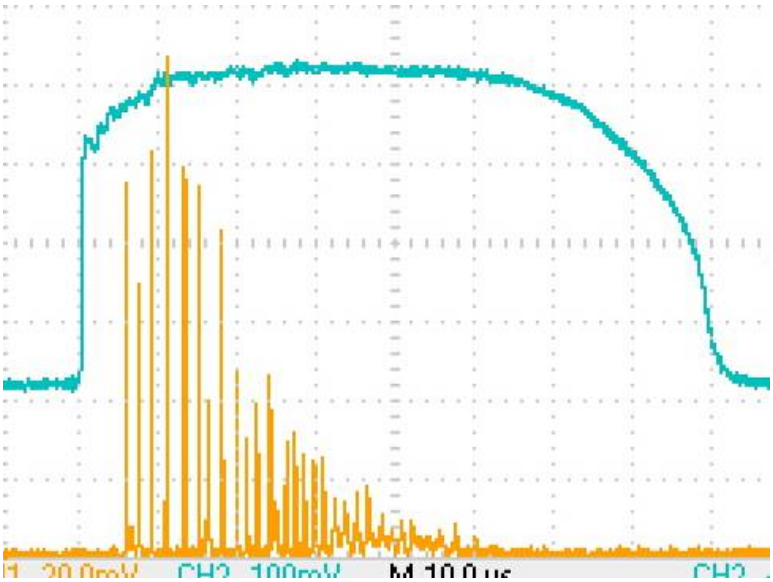

Figure 3-24: Temporal Profile of the Cr^{3+}:LiSAF Laser Pulse (Cyan) and the Ho^{3+}:fluoroindate Laser Pulse (Orange) at Maximum Output Energy.

The set-up was not optimized for a 30-mm long laser material. Nevertheless we obtained, for the first time to our knowledge, a laser emission from a Ho^{3+}:fluoroindate glass. We think that this is the first step towards a pulsed mid-infrared fiber laser based on this material.

3.5 REFERENCES

[1] Barnes, N.P. and Allen, R. Room temperature Dy:YLF laser operation at 4.34 mm, IEEE Journal of Quantum Electronics v. 27, 277-282 (1991).

[2] Jackson, S.D. Continuous wave 2.9 μm dysprosium-doped fluoride fiber laser, Appl. Phys. Lett. 83, 1316 (2003).

[3] Schneider, J. Fluoride fibre laser operating at 3.9 μm, *Electron. Lett.*, Vol. 31, pp. 1250-1251 (1995).

[4] Schneider, J., Carbonnier, C. and Unrau, U. Characterization of a Ho^{3+}-doped fluoride fiber laser with a 3.9-μm emission wavelength, *Appl. Opt.*, Vol. 36, pp. 8595-8600 (1997).

[5] Eichhorn, M. Fluorescence reabsorption and its effects on the local effective excitation lifetime, Appl Phys B 369-377 (2009).

[6] Quimbye, R.S., Shaw, L.B., Sanghera, J.S. and Aggarwal, I.D. Modeling of Cascade Lasing in Dy:Chalcogenide Glass Fiber Laser With Efficient Output at 4.5 μm, IEEE Photonics Technology Letters 20, 123-125 (2007).

[7] Jackson, S.D. High-power and Highly efficient diode-cladding-pumped holmium-doped fluoride fiber laser operating at 2.94 μm, Opt. Lett. 34, 2327-2329 (2009).

[8] Li, J., Hudson, D.D. and Jackson, S.D. High-power diode-pumped fiber laser operating at 3 μm, Opt. Lett. 36, 3642-3644 (2011).

[9] Schneider, J., Carbonnier, C. and Unrau, U.B. Characterization of a Ho^{3+}-doped fluoride fiber laser with a 3.9-μm emission wavelength, Appl. Opt. 36, 8595-8599 (1997).

[10] Eichhorn, M. Quasi-three-level solid-state lasers in the near and mid infrared based on trivalent rare earth ions, Applied Physics B 93, 269-316 (2008).

[11] Barnes, N.P., Walsh, B.M. and Filer, E.D. Ho:Ho upconversion: applications to Ho lasers, J. Opt. Soc. Am. B 20, 1212-1219 (2003).

[12] Jackson, S.D. Towards high-power mid-infrared emission from a fiber laser, Nature Photonics 6, 423-431 (2012).